Antarctic ice dynamics amplified by Northern Hemisphere sea-level forcing

Antarctic ice dynamics amplified by Northern Hemisphere sea-level forcing

Authors: Natalya Gomez*[1], Michael E. Weber[2], Peter U. Clark[3.4], Jerry X. Mitrovica[5], Holly K. Han[1]

1. Department of Earth and Planetary Sciences, McGill University, Montreal, QC, H3A 0E8, Canada
2. Department of Geochemistry and Petrology, Institute for Geosciences, University of Bonn, Bonn, Germany
3. College of Earth, Ocean, and Atmospheric Sciences, Oregon State University, Corvallis, OR, USA
4. School of Geography and Environmental Sciences, University of Ulster, Coleraine, Northern Ireland, UK
5. Department of Earth and Planetary Sciences, Harvard University, Cambridge, MA, USA

Abstract:

A long-standing hypothesis for synchronous global ice-sheet evolution on orbital timescales invokes an interhemispheric sea level forcing, whereby sea-level rise due to ice loss in the Northern Hemisphere (NH) in response to insolation and greenhouse gas forcing causes grounding line retreat of marine-based sectors of the Antarctic Ice Sheet (AIS)[1-3]. Recent evidence indicates that the AIS experienced substantial millennial-scale variability during and after the last deglaciation[4-7], further suggesting a possible sea-level forcing. Global sea-level change from ice-sheet mass loss is strongly nonuniform[8], however, suggesting that the response of AIS grounding lines to NH sea-level forcing is likely more complicated than previously considered[1,2,6]. Here we show, using a coupled ice sheet - global sea-level model, that a large or rapid NH sea-level forcing during

deglaciation reduces or exceeds the sea-level fall at AIS grounding lines driven by the gravitational and deformational effects of AIS mass loss, enhancing grounding line retreat and associated AIS mass loss. In contrast, during NH glaciation, the sea-level forcing acts to enhance grounding-line advance. We find that including these effects causes NH sea-level forcing to increase AIS volume during the Last Glacial Maximum (LGM, ~26-20 ka) and triggers an earlier retreat and millennial scale variability through the last deglaciation, consistent with geologic reconstructions of LGM AIS extent and subsequent ice-sheet retreat and relative sea-level change in Antarctica[3-7,9,10].

Main

Several mechanisms exist to explain near-synchronous interhemispheric climate changes on orbital timescales despite opposite insolation forcing[11,12]. Synchronous changes in surface climate, however, cannot explain synchronous changes in the Northern Hemisphere (NH) and Antarctic ice sheets[3,13] because they would have induced opposing ice-sheet surface mass balance (SMB) responses, with warming climate over the AIS leading to a more positive SMB[3]. In the absence of surface melting, mechanisms that impact the primary controls on Antarctic Ice Sheet (AIS) mass balance (basal melting of buttressing ice shelves and ice discharge across grounding lines of marine-based sectors) are thus required for ice-sheet synchronization.

Studies have shown that an increase in subsurface warming from changes in ocean circulation contributes to AIS deglaciation[4,5,14,15]. Marine-based sectors of ice sheets are also vulnerable to sea-level change at their grounding lines, whereby a local sea-level fall may slow or stabilize grounding line retreat or initiate or enhance its advance, while a sea-level rise may slow grounding line advance or initiate or enhance its retreat[16,17].

Previous work suggested that sea-level rise from deglaciation of NH ice sheets triggered retreat of grounding lines of the AIS, thus synchronizing ice-sheet variability globally[1,2,18,19]. Well-dated geologic records of AIS fluctuations support synchronization on orbital timescales[3,13] and identify linkages between periods of sea-level rise and millennial-scale AIS variability during the last deglaciation, 20 to 9 thousand years ago (ka). For example, deep-sea sediments from Scotia Sea's Iceberg Alley record eight discrete episodes of increased flux of iceberg-rafted debris (IBRD) originating from the AIS during the last deglaciation[4]. Three of these AIS Discharge (AID) events occurred at

60 the same time as well-documented periods of sea-level rise, suggesting a possible
61 linkage: AID 7 corresponds to the onset of deglacial sea-level rise ~19.5-19 ka[3,20], AID 6
62 corresponds to Meltwater Pulse 1A (MWP-1A) ~14.5 ka[21], and AID 2 corresponds to an
63 acceleration of sea-level rise during the early Holocene starting at ~11.5 ka [22,23].
64 Additional evidence for this dynamic ice-sheet behavior comes from isotopic records
65 from a horizontal ice core in the Patriot Hills of the Weddell Sea Embayment[6], which
66 suggest that the ice surface in that region lowered by ≥600 m during AID 6 and around
67 AID 2. Finally, marine records from the Ross Sea identify a step-wise retreat of the West
68 AIS grounding line coincident with AID 6 and AID 2 (ref. [7]). The IBRD record suggests
69 that after AID 1 from ~10.4-9 ka, there was a substantial reduction in the amplitude of
70 iceberg-flux variability over the past 8 kyr[24], and global mean sea level (GMSL)
71 experienced only decimeter-scale changes over the last 6 kyr[25]. Current uncertainties in
72 these far-field sea level reconstructions and the age model for Antarctic IBRD cores[4]
73 preclude a determination of the relative phasing between the AID events and the sea-level
74 change associated with NH ice melting, but modeling can provide insight into the
75 mechanisms that lead to these observed changes.
76 Here we investigate possible interhemispheric ice-sheet coupling through sea-level
77 change over the last 40 ky and assess its impact on AIS evolution and behavior. We
78 model the evolution of the AIS and global sea-level changes using the Pennsylvania State
79 University (PSU) 3-D ice-sheet model coupled to a gravitationally self-consistent global
80 sea-level model that includes viscoelastic deformation of the solid Earth, rotational
81 feedbacks, and migrating shorelines[26] (see Methods).
82

Deglacial sea-level change in Antarctica

Fig. 1a shows ice loss since 21 ka from the AIS as calculated in a coupled ice sheet – sea level model simulation and from NH ice sheets derived from the ICE5G ice history[27]. The AIS simulation is based on parameters identified in a large ensemble analysis as best-fitting a range of paleo and modern data constraints[28], and is characterized by a GMSL equivalent mass loss of 5 m from the AIS, with 107 m from the NH in ICE5G (see Methods and Extended Data Fig. 1 for results of simulations with a larger AIS contribution to GMSL). Peak sea-level fall is predicted to reach 150 m in previously glaciated regions in Antarctica while the bedrock deepens in the interior of Antarctica and sea level rises by 150 m in the surrounding ocean (Fig. 1b). Mass loss from NH ice sheets contributes a sea-level rise that increases from 80 m in East Antarctica to 130 m in West Antarctica (Fig. 1c), in agreement with previous work[3]. This sea-level gradient is driven by a shift of the Earth's rotation axis towards North America in the NH, where most ice is being lost (Fig. 1a), and towards East Antarctica in the Southern Hemisphere, driving lower than average sea-level rise in these regions and higher than average sea-level rise in the opposing quadrants of the Earth's surface (which include West Antarctica and Eurasia). In contrast, AIS mass loss drives a sea-level fall of up to 300 m in previously glaciated regions of Antarctica due to gravitationally driven lowering of the sea surface and viscoelastic uplift of the solid Earth under the areas of mass loss (Fig. 1d). The sea-level fall associated with local AIS loss thus dominates the total Antarctica signal in these areas, but sea-level rise from the much larger NH ice-mass loss substantially decreases the geographic spread and magnitude of sea-level fall at Antarctic grounding lines over the last deglaciation (compare Figs. 1b, d).

AIS response to NH sea-level forcing

To quantify how sea-level changes associated with NH ice-sheet variations (Figs. 1c, 2a) influenced AIS dynamics leading up to the Last Glacial Maximum (LGM, ~26-20 ka[13]) and during the last deglaciation, we compare AIS mass changes predicted from model simulations that include the evolution of the NH ice sheets prescribed from five ice-history reconstructions[27,29-31] to those predicted from a simulation in which the NH ice sheets remain fixed in their initial configuration at 40 ka and do not contribute to sea-level changes in Antarctica over the simulation (Fig. 2b; Extended Data Figs 8; Methods). In the simulations, NH ice growth leading up to the LGM contributes a sea-level fall beginning at ~30 ka (Fig. 2a), which drives additional AIS growth at ~28 ka (Fig. 2b). This growth occurs primarily in the Antarctic Peninsula and Weddell Sea regions (Extended Data Figs. 2c and 3, at 20 ka; Extended Data Fig. 4) and is consistent with evidence for when ice reached its LGM extent in these regions[3].

During the last deglaciation, sea-level rise from NH ice-sheet retreat (Fig. 2a) significantly enhances the magnitude and rate of AIS mass loss from 15 ka onward (Fig. 2b, Extended Data Figs. 2 and 3), whereas the simulation with no NH sea-level forcing is characterized by net AIS growth over much of the same period (Fig. 2b). In particular, with fixed NH ice, extensive grounded ice remains in the Weddell Sea and, to a lesser extent, the Ross Sea regions until the present day (Extended Data Figs. 2 and 3), whereas including a NH sea-level forcing causes these regions to completely deglaciate, reaching a modern Antarctic ice volume close to the observed (2.69×10^7 km^3; ref. [32]). We note that differences in AIS evolution are greatest in the Weddell Sea region (Extended Data Fig. 4) where the largest sea-level forcing is predicted from NH ice-mass loss (Fig. 1c). We

129 have highlighted the sensitivity of the ice sheet to this geographic variability in Extended
130 Data Fig. 7.
131
132 **MWP-1A and early Holocene ice loss**
133 Our simulations suggest that an increase in AIS mass loss after 15 ka driven by NH
134 sea-level forcing contributed to Meltwater Pulse 1A (MWP-1A) ~14.5 ka and support an
135 Antarctic source for early Holocene acceleration in sea-level rise (Bard et al., 2016) (Fig.
136 2). Specifically, the AIS simulations that include a NH sea-level forcing during the
137 deglaciation show distinct corresponding periods of rapid mass loss (Figs. 2b, 3a) during
138 and after the time of these two episodes of rapid sea-level rise. This behavior may thus
139 explain the large increases in IBRD flux in Iceberg Alley (AID events 6, 2 and 1, ref. [4];
140 Fig. 2c) and the evidence for mass loss from the Weddell Sea[6] and Ross Sea[7] regions at
141 these times. Alternate physical processes (such as ocean and atmospheric forcing) must
142 be sought to explain the remaining AID events during the last deglaciation[4].
143 In the case of MWP-1A, the AIS experiences more extensive mass loss (Figs. 2b,
144 3a, and Extended Data Fig. 5) in the simulations in which NH ice sheets evolve relative
145 to the simulation where they are fixed and AIS mass loss is driven only by climate
146 forcing on the ice sheet[14] (Figs. 3a-c). The net volume of ice lost in the latter simulation
147 over this period is 2.5–3 times less than predicted in the former across the range of
148 evolving NH ice histories we consider. In the case of the early Holocene, including NH
149 sea-level forcing increases the rate of AIS mass loss by up to a factor of ~4 starting at
150 ~11.5 ka (Fig. 3a), the time of MWP-1B suggested by the far-field Barbados sea-level
151 record[23] and AID 2 (ref. [4]). This mass loss continues throughout AID 1 until between 9.5-

9 ka (Figs. 2, 3, Extended data Fig. 5), with substantial grounding line retreat in both the Ross Sea and Weddell Sea regions (compare Figs. 3d and e). The amplified AIS response during the early Holocene occurs regardless of whether there is an acceleration in NH ice loss during that time or not (compare Extended Data Fig. 5a with ICE5G[27] and Figs. 5b-c with ICE6G[31] and ANU[30]) and it is consistent with the hypothesis of a significant or dominant Antarctic source for acceleration in GMSL rise[31,33] during this period (see also Extended Data Fig. 6).

We have confirmed that the general behavior evident in Figs. 2 and 3 holds for coupled model simulations using a range of Earth and ice-model parameters (Extended Data Figs. 1 and 8). The largest difference is found in simulations with less basal sliding. These simulations result in a larger LGM ice sheet (Extended Data Fig. 1) with AIS growth in the first half of the simulations being less sensitive to NH ice growth and the associated sea-level fall than simulations with more basal sliding. The concordance between the two simulations with less basal sliding is likely because the AIS margin nearly reaches its maximum possible extent at the continental shelf edge in both cases.

Comparison to geologic records

We next consider local ice-sheet and sea-level changes in the Ross Sea region where there are reconstructions of relative sea level[9,34] (Southern Scott Coast, Site S in Fig. 4a), grounding line migration[7], and changes in ice-surface elevation (Site 1 in Fig. 4; other sites in the Ross and Weddell Sea regions are discussed in Extended Data Figs. 10-11)[35] that provide a test of the local response to NH sea-level forcing. When this forcing is included, deglaciation of the region is predicted to begin in the early Holocene (Fig.

175 4a) with regional ice thinning occurring from 11 to 8 ka (blue, black and cyan curves
176 show thinning at both Sites S and 1 in Fig. 4b). This model result is consistent with
177 observations of ice-surface lowering at Site 1 (ref. [35]) (error bars, Fig. 4b; nearby Sites 3-
178 5 which are just outside of the region of substantial ice thinning, are discussed in
179 Extended Data Fig. 11), a major grounding line retreat of ≥200 km in the Ross Sea[7] and a
180 peak IBRD flux during AID events 2 and 1 (ref. [4]). In contrast, this retreat takes place
181 from 10 to 6 ka at Sites S and 1 when NH sea-level forcing is not included in the
182 simulation (Fig. 4b), which is also inconsistent with a relatively low observed IBRD flux
183 from ~8.5 ka onward[24] (grey line, Fig. 4b).

184 At Site S, local sea-level change during the deglacial phase is initially dominated
185 by NH-driven sea-level rise, but as local ice loss begins (~11 ka) the gravitational and
186 deformational effects associated with this ice loss dominate the local sea-level change
187 (Fig. 4c). When the NH-driven sea-level forcing is excluded (Fig. 4c), relative sea-level
188 fall is predicted to begin later, at ~9 ka, coincident with local ice loss for this simulation
189 shown in Fig. 4b, and there is almost no change in relative sea level prior to 10 ka. The
190 oldest relative sea-level indicators from this area (~6.5 ka; Fig. 4c) are more consistent
191 with the lower relative sea level predicted by the simulations that include the NH sea-
192 level forcing, but older indicators are needed to clearly corroborate this, especially given
193 the uncertainty in local viscoelastic Earth structure.

194

195 **Summary**

196 We conclude that geographically variable sea-level changes around Antarctica
197 driven by NH ice-sheet changes strongly modulated AIS growth and decay. In particular,

NH ice growth leading up to the LGM causes local sea-level fall and further AIS growth in our simulations, yielding a higher peak AIS volume at the LGM than without this forcing. Conversely, NH ice loss during the last deglaciation produces a sea-level rise of 80–130 m in Antarctica in our model, driving earlier, greater and more rapid AIS retreat that is in better agreement with geological evidence than predictions that omit this forcing. The simulations indicate that the Weddell Sea region of the AIS was subject to the largest sea-level changes driven by NH ice changes, suggesting that ice-mass changes in this region were particularly sensitive to this far-field sea-level forcing. Finally, simulations with NH sea-level forcing predict increases in AIS mass flux during MWP-1A and the early Holocene, consistent with multiple lines of geologic evidence for AIS mass loss at these times.

References:

1 Denton, G. H. & Hughes, T. J. Milankovitch theory of ice ages: Hypothesis of ice-sheet linkage between regional insolation and global climate. *Quaternary Research* **20**, 125-144 (1983).

2 Huybrechts, P. J. Sea-level changes at the LGM from ice-dynamic reconstructions of the Greenland and Antarctic ice sheets during the glacial cycles. *Quaternary Science Reviews* **21**, 203-231 (2002).

3 Weber, M. E. *et al.* Interhemispheric ice-sheet synchronicity during the Last Glacial Maximum. *Science* **334**, 1265-1269, doi:10.1126/science.1209299 (2011).

4 Weber, M. E. *et al.* Millennial-scale variability in Antarctic ice-sheet discharge during the last deglaciation. *Nature* **510**, 134-138, doi:10.1038/nature13397 (2014).

5 Golledge, N. R. *et al.* Antarctic contribution to meltwater pulse 1A from reduced Southern Ocean overturning. *Nature Communications* **5**, 5107, doi:10.1038/ncomms6107 (2014).

6 Fogwill, C. J. *et al.* Antarctic ice sheet discharge driven by atmosphere-ocean feedbacks at the Last Glacial Termination. *Scientific Reports* **7**, 39979, doi:10.1038/srep39979 (2017).

7 Bart, P. J., DeCesare, M., Rosenheim, B. E., Majewski, W. & McGlannan, A. A centuries-long delay between a paleo-ice-shelf collapse and grounding-line

retreat in the Whales Deep Basin, eastern Ross Sea, Antarctica. *Scientific Reports* **8**, 12392, doi:10.1038/s41598-018-29911-8 (2018).

8 Milne, G. A. & Mitrovica, J. X. Searching for eustasy in deglacial sea-level histories. *Quaternary Science Reviews* **27**, 2292-2302, doi:10.1016/j.quascirev.2008.08.018 (2008).

9 Hall, B. L. & Denton, G. H. New relative sea‐level curves for the southern Scott Coast, Antarctica: evidence for Holocene deglaciation of the western Ross Sea. *Journal of Quaternary Science* **14**, 641-650 (1999).

10 Fogwill, C. J. *et al.* Southern Ocean carbon sink enhanced by sea-ice feedbacks at the Antarctic Cold Reversal. *Nature Geoscience*, doi:10.1038/s41561-020-0587-0 (2020).

11 Kawamura, K. *et al.* Northern Hemisphere forcing of climatic cycles in Antarctica over the past 360,000 years. *Nature* **448**, 912-916 (2007).

12 Huybers, P. & Denton, G. Antarctic temperature at orbital timescales controlled by local summer duration. *Nature Geoscience* **1**, 787-792 (2008).

13 Clark, P. U. *et al.* The last glacial maximum. *Science* **325**, 710-714 (2009).

14 Pollard, D., Chang, W., Haran, M., Applegate, P. & DeConto, R. Large ensemble modeling of the last deglacial retreat of the West Antarctic Ice Sheet: comparison of simple and advanced statistical techniques. *Geoscientific Model Development* **9**, 1697-1723, doi:10.5194/gmd-9-1697-2016 (2016).

15 Clark, P. U. *et al.* Oceanic forcing of penultimate deglacial and last interglacial sea-level rise. *Nature* **577**, 660-664 (2020).

16 Weertman, J. Stability of the junction of an ice sheet and an ice shelf. *Journal of Glaciology* **13**, 3, doi:10.1017/s0022143000023327 (1974).

17 Schoof, C. Ice sheet grounding line dynamics: Steady states, stability, and hysteresis. *Journal of Geophysical Research* **112**, F03S28-19, doi:10.1029/2006JF000664 (2007).

18 Denton, G. H., Hughes, T. J. & Karlén, W. Global ice-sheet system interlocked by sea level. *Quaternary Research* **26**, 3-26 (1986).

19 Tigchelaar, M., Timmermann, A., Friedrich, T., Heinemann, M. & Pollard, D. Nonlinear response of the Antarctic Ice Sheet to late Quaternary sea level and climate forcing. *Cryosphere* **13** (2019).

20 Yokoyama, Y., Lambeck, K., De Deckker, P., Johnston, P. & Fifield, L. K. Timing of the Last Glacial Maximum from observed sea-level minima. *Nature* **406**, 713-716, doi:10.1038/35021035 (2000).

21 Deschamps, P. *et al.* Ice-sheet collapse and sea-level rise at the Bølling warming 14,600 years ago. *Nature* **483**, 559-564, doi:10.1038/nature10902 (2012).

22 Bard, E., Hamelin, B. & Delanghe-Sabatier, D. Deglacial Meltwater Pulse 1B and Younger Dryas sea levels revisited with boreholes at Tahiti. *Science* **327**, 1235-1237, doi:10.1126/science.1180557 (2010).

23 Abdul, N. A., Mortlock, R. A., Wright, J. D. & Fairbanks, R. G. Younger Dryas sea level and meltwater pulse 1B recorded in Barbados reef crest coral Acropora palmata. *Paleoceanography* **31**, 330-344, doi:10.1002/2015PA002847 (2016).

24 Bakker, P., Clark, P. U., Golledge, N. R., Schmittner, A. & Weber, M. E. Centennial-scale Holocene climate variations amplified by Antarctic Ice Sheet discharge. *Nature* **541**, 72-76, doi:10.1038/nature20582 (2017).
25 Hallmann, N. *et al.* Ice volume and climate changes from a 6000 year sea-level record in French Polynesia. *Nature Communications* **9**, 285, doi:10.1038/s41467-017-02695-7 (2018).
26 Gomez, N., Pollard, D. & Mitrovica, J. X. A 3-D coupled ice sheet – sea level model applied to Antarctica through the last 40 ky. *Earth and Planetary Science Letters* **384**, 88-99 (2013).
27 Peltier, W. R. Global glacial isostasy and the surface of the ice-age Earth: the ICE-5G (VM2) model and GRACE. *Annual Review of Earth and Planetary Sciences* **32**, 111, doi:10.1146/annurev.earth.32.082503.144359 (2004).
28 Pollard, D., Gomez, N. & DeConto, R. M. Variations of the Antarctic Ice Sheet in a coupled ice sheet-Earth-sea level model: Sensitivity to viscoelastic Earth properties. *Journal of Geophysical Research: Earth Surface* **122**, 2124-2138, doi:10.1002/2017JF004371 (2017).
29 Tarasov, L., Dyke, A. S., Neal, R. M. & Peltier, W. R. A data-calibrated distribution of deglacial chronologies for the North American ice complex from glaciological modeling. *Earth and Planetary Science Letters* **315**, 30-40 (2012).
30 Lambeck, K., Rouby, H. & Purcell, A. Sea level and global ice volumes from the Last Glacial Maximum to the Holocene. *Proceedings of the National Academy of Sciences* **111**, 15296, doi:10.1073/pnas.1411762111 (2014).
31 Peltier, W. R., Argus, D. F. & Drummond, R. Space geodesy constrains ice age terminal deglaciation: The global ICE-6G_C (VM5a) model. *Journal of Geophysical Research: Solid Earth* **120**, 450-487 (2015).
32 Fretwell, P. *et al.* Bedmap2: Improved ice bed, surface and thickness datasets for Antarctica. *The Cryosphere* 7.1, 375-393 (2013).
33 Bard, E., Hamelin, B., Deschamps, P. & Camoin, G. Comment on "Younger Dryas sea level and meltwater pulse 1B recorded in Barbados reefal crest coral Acropora palmata" by N. A. Abdul et al. *Paleoceanography* **31**, 1603-1608, doi:10.1002/2016PA002979 (2016).
34 Briggs, R. D. & Tarasov, L. How to evaluate model-derived deglaciation chronologies: a case study using Antarctica. *Quaternary Science Reviews* **63**, 109-127, doi:10.1016/j.quascirev.2012.11.021 (2013).
35 Jones, R., Whitehouse, P., Bentley, M., Small, D. & Dalton, A. Impact of glacial isostatic adjustment on cosmogenic surface-exposure dating. *Quaternary Science Reviews* **212**, 206-212 (2019).

Main Text Figure Captions:

Figure 1: Contributions to deglacial sea-level changes in Antarctica. (a) Grounded ice-thickness changes in meters since 21 ka in the coupled ice sheet – sea level simulation, based on the ICE5G[27] ice history in the NH and the dynamic ice-sheet model

in Antarctica. (b) Predicted total relative sea-level change, in meters, since 21 ka in Antarctica. (c) Component of frame (b) associated with ice-cover changes in the NH in the ICE5G[27] ice history, computed from a simulation with the sea-level model alone. (d) Difference between frames (b) and (c), showing changes in relative sea level associated with Antarctic ice-cover changes.

Figure 2: Timing of NH sea level forcing and its influence on Antarctic ice volume changes. (a) Prescribed changes in NH ice volume from the ICE5G[27] (solid black line), ICE6GC[31] (dashed black line) and the ANU[30] (cyan) ice histories, as well as two composite ice histories in which ice cover over North America and Greenland in ICE5G has been replaced by GLAC1D[29] regional ice histories (blue lines). Blue vertical bands indicate the timing of MWP-1A[21] and MWP-1B[22]. (b) Changes in Antarctic ice volume predicted in simulations with fixed (red line) and evolving NH ice taken from the ice histories shown in frame (a) (blue, cyan and black lines). Green vertical bands indicate periods during MWP-1A and the earth Holocene in the model simulations that are examined in the text and other figures. (c) Iceberg rafted debris flux from sediment cores in Iceberg Alley[4] adopting the AIC 2012 model (see Methods and Extended Data Figure 9). Vertical red bands indicate the timing of AIS Discharge (AID) events, 1, 2 and 6 as labeled, and horizontal blue bands indicate the timing of Last Glacial Maximum extent in Weddell Sea (LGM WS)[3].

Figure 3: Enhanced Antarctic ice loss during MWP-1A and the early Holocene. (a) Rate of change of Antarctic ice volume, including grounded and floating ice, calculated as a 100-year running mean, predicted from simulations including (black line) and excluding (red line) NH ice-cover changes. The black line and shading represent the mean and standard deviation of predictions generated with the five ice histories described in the text. (b–e) Change in Antarctic ice thickness during (b,c) MWP-1A from 14.5–13.5 ka, and (d,e) the early Holocene starting from the time of MWP-1B from 11.5-9 ka. Frames (b,d) are based on simulations which include ice mass flux from the NH from the ICE5G ice history. These simulations predict Antarctica ice loss equivalent to a GMSL rise of 1.14 m and 1.95 m across the MWP-1A and early Holocene time windows, respectively. Frames (c,e) are generated from simulations in which NH ice sheets remain fixed throughout the simulation. Grey-blue and black lines in (b–e) indicate the grounding line position at the start and end of the time interval, respectively.

Figure 4: Agreement of predicted sea-level and ice-cover changes with geological records in the Ross Sea sector. (a) Predicted Antarctic ice cover in the simulation that includes NH ice from ICE5G[27] at snapshots in time as the Ross Sea region deglaciates. (b) Predicted ice-thickness above modern thickness in meters at Site S, indicated by the red dots in (a), and Site 1 from ref. [35], indicated by the blue dots in (a), for simulations in which NH ice cover is evolving according to ICE5G[27] and ANU[30] ice histories (black and cyan lines for Site S, solid blue line for Site 1) and fixed (red line for Site S, dashed blue line for Site 1). Error bars show cosmogenic exposure age data with 2σ uncertainty from ref. [35] at Site 1. The grey time series is the recorded flux of Antarctic iceberg-rafted debris (IBRD) in grains/yr/cm^3 shown in Fig. 2c, and red vertical bands indicate AIDs 1 and 2. (c) Predictions of relative sea-level change at Site S for the cases of evolving

(black and cyan lines) and fixed (red line) NH ice cover. Dashed black and cyan lines in (c) indicate the contribution to GMSL change from NH ice-cover prescribed in the ICE5G[27] (solid blue) and ANU[30] (dashed blue) ice histories. Black markers with 2σ error bars show two-way (circles) or lower-bound (triangle) relative sea-level constraints from ref. [9].

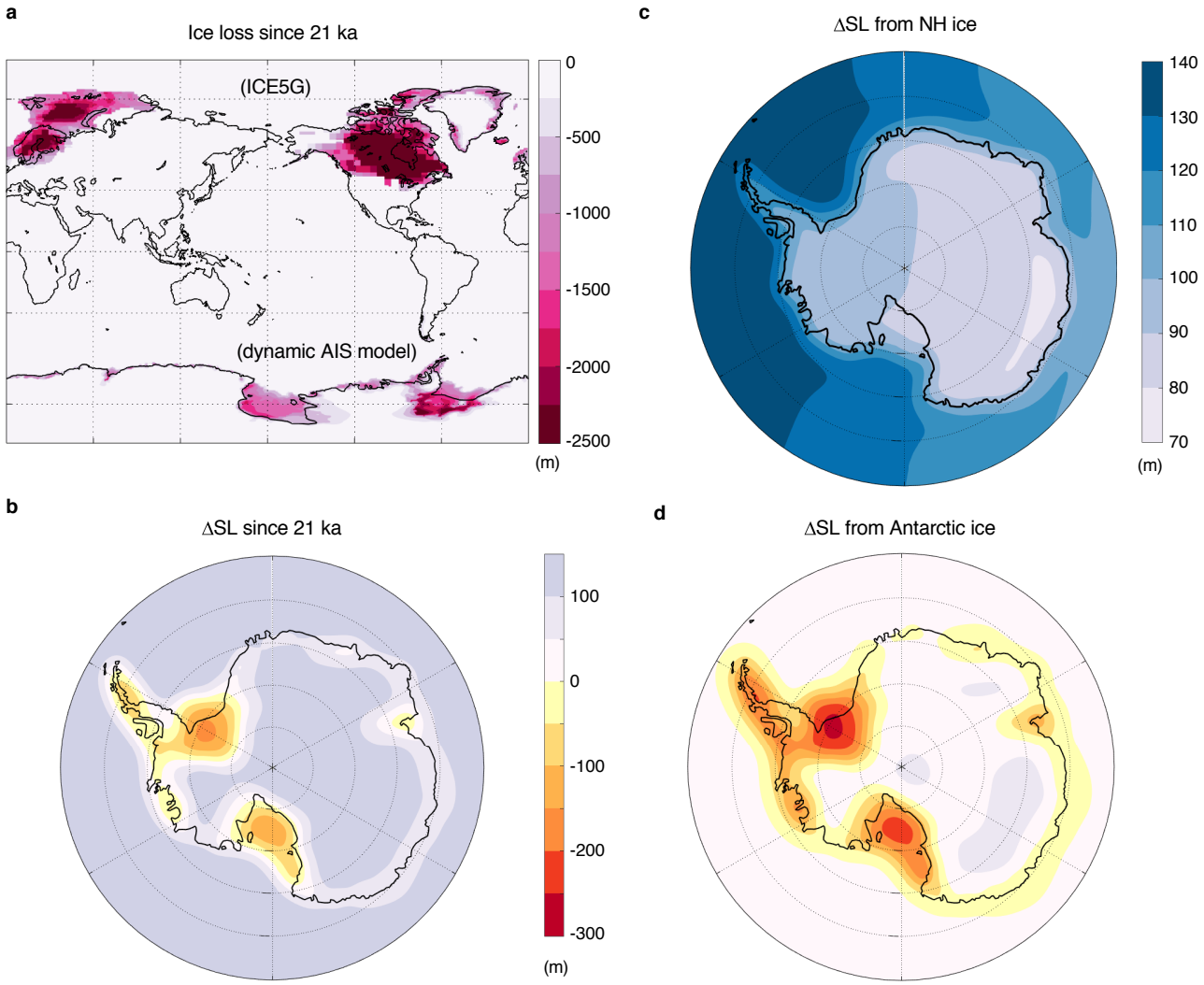
a
Ice loss since 21 ka
(ICE5G)
(dynamic AIS model)
0
-500
-1000
-1500
-2000
-2500
(m)
c
ΔSL from NH ice
140
130
120
110
100
90
80
70
(m)
b
ΔSL since 21 ka
100
0
-100
-200
-300
(m)
d
ΔSL from Antarctic ice

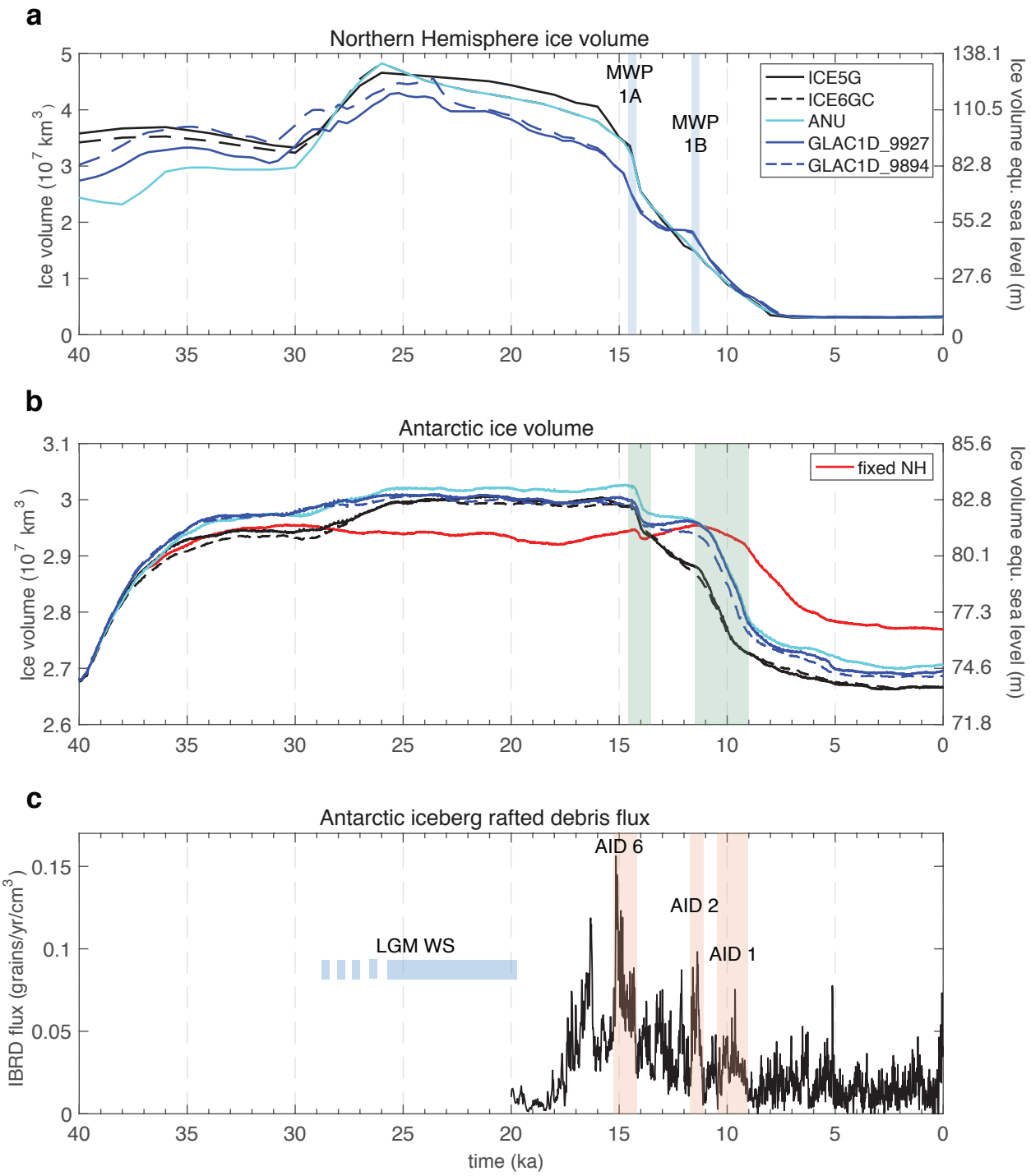
a
Northern Hemisphere ice volume
MWP 1A
MWP 1B
ICE5G
ICE6GC
ANU
GLAC1D_9927
GLAC1D_9894
Ice volume (10^7 km^3)
Ice volume equ. sea level (m)
b
Antarctic ice volume
fixed NH
Ice volume (10^7 km^3)
Ice volume equ. sea level (m)
c
Antarctic iceberg rafted debris flux
AID 6
AID 2
AID 1
LGM WS
IBRD flux (grains/yr/cm^3)
time (ka)

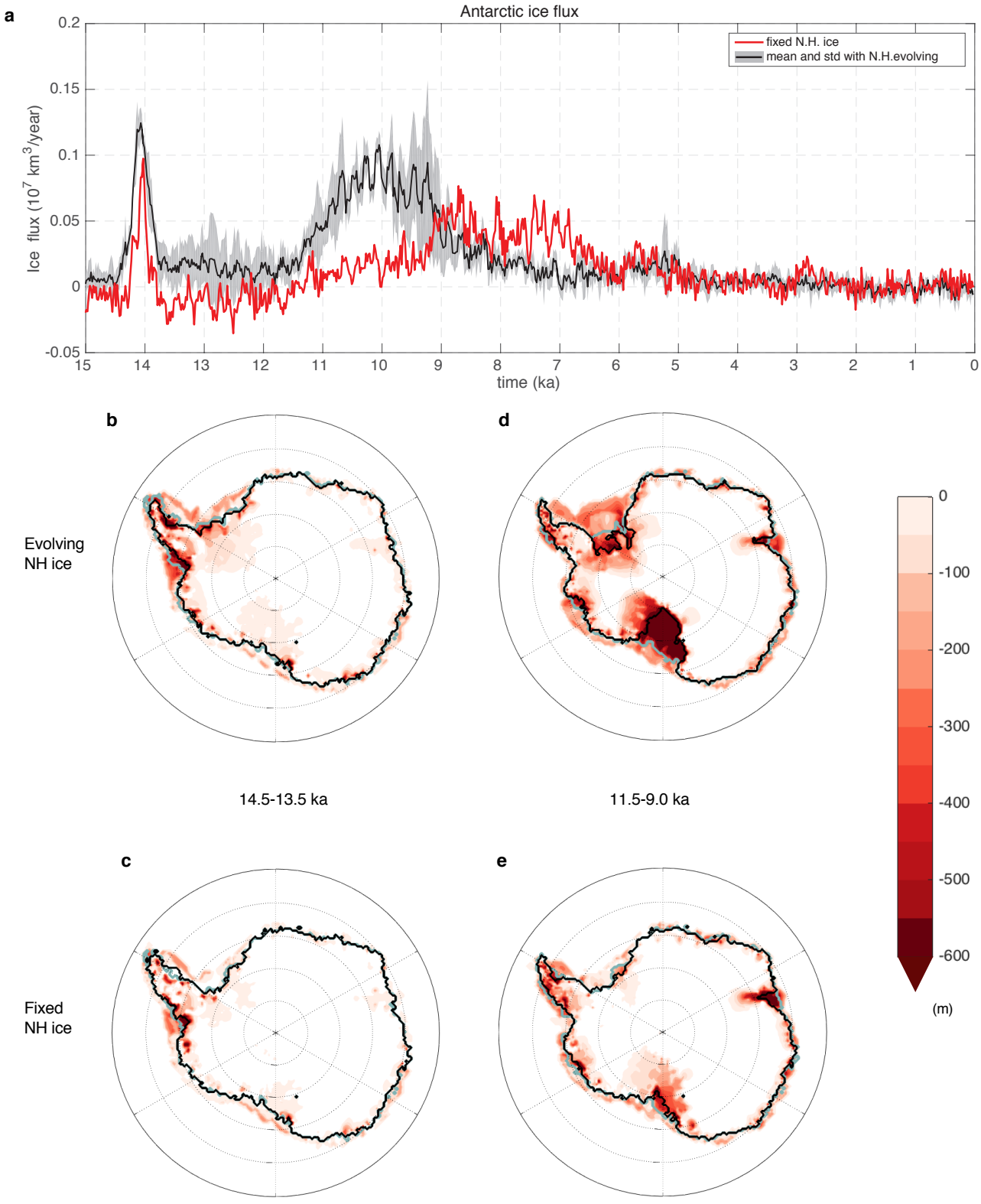
a
Antarctic ice flux
fixed N.H. ice
mean and std with N.H.evolving
Ice flux (10^7 km^3/year)
time (ka)
b
d
Evolving
NH ice
14.5-13.5 ka
11.5-9.0 ka
c
e
Fixed
NH ice
0
-100
-200
-300
-400
-500
-600
(m)

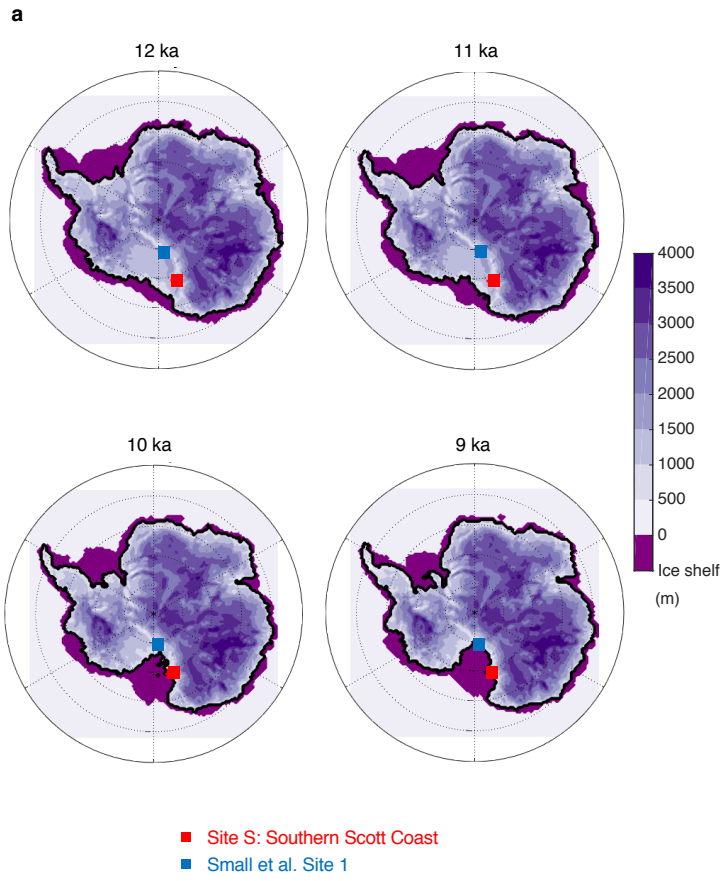
a
12 ka
11 ka
10 ka
9 ka
4000
3500
3000
2500
2000
1500
1000
500
0
Ice shelf
(m)
Site S: Southern Scott Coast
Small et al. Site 1

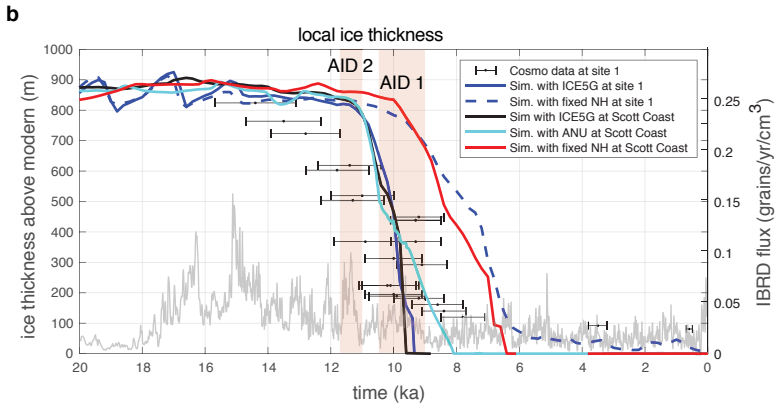
b
local ice thickness
AID 2
AID 1
Cosmo data at site 1
Sim. with ICE5G at site 1
Sim. with fixed NH at site 1
Sim with ICE5G at Scott Coast
Sim. with ANU at Scott Coast
Sim. with fixed NH at Scott Coast
ice thickness above modern (m)
IBRD flux (grains/yr/cm3)
time (ka)

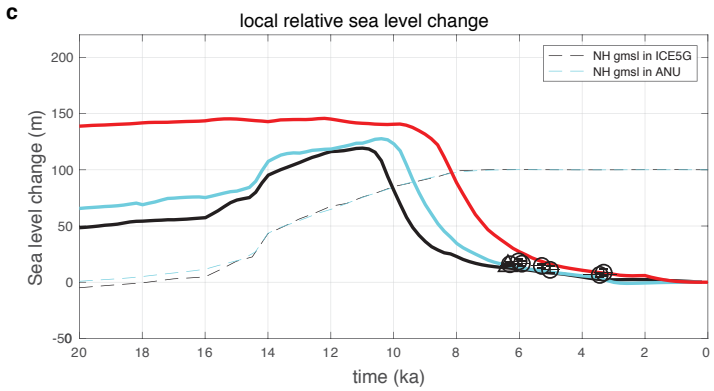
c
local relative sea level change
NH gmsl in ICE5G
NH gmsl in ANU
Sea level change (m)
time (ka)

Methods:

Coupled ice sheet - sea level modeling

The evolution of the AIS and global sea-level changes was modeled using the coupled ice sheet – sea level model developed and described in detail in ref. [26] and applied in refs. [36] and [28]. The model consists of the PSU 3-D ice-sheet model[37] coupled to a gravitationally self-consistent global sea-level model that includes viscoelastic deformation of the solid Earth, rotational feedbacks onto sea level and migrating shorelines[38,39].

PSU 3-D is a finite difference, ice sheet – ice shelf model that adopts hybrid combinations of the scaled Shallow-Ice and Shallow-Shelf equations[40,41] to treat ice dynamics, and includes grounding-line migration through a parameterization of flux across the grounding line[17]. This grounding line treatment performs reasonably well in comparison with higher order ice-sheet models[42] and facilitates the computational feasibility of glacial-interglacial timescale simulations. Basal sliding in the model is treated with a standard Weertman-type sliding law and basal sliding coefficients are determined through inverse fitting to ice thickness under regions with grounded ice in the modern[43]. In modern oceanic regions, where basal sliding is relatively unconstrainted, the coefficient is set to 10^{-5} m a^{-1} Pa^{-2} in simulations presented in the main text and to 10^{-6} m a^{-1} Pa^{-2} in additional simulations summarized in Extended Data Fig. 1, representing the range identified in ref. [28] to best fit a suite of paleo ice-sheet and sea-level constraints. Note that alternate basal sliding laws have been proposed[44,45] but model treatments remain unverified by observations and should be explored further in future work. Other ice model parameters such as the calving coefficient and ocean melt factor are similarly

399 set to the best fitting values identified in refs. [14] and [28]. Here and in these references,
400 atmospheric climate forcing was applied by perturbing modern climatology (ALBMAP[46])
401 to mimic past conditions according to a deep-sea $\delta^{18}O$ stack[47]. Sub-ice shelf melt rates
402 are determined through a parameterization that depends on subsurface oceanic
403 temperatures from ref. [48] with sensitivity inferred from the aforementioned large
404 ensemble model-data comparisons[28]. We note that the best fitting simulations in these
405 studies produce a relatively small contribution from the Antarctic to sea level over the
406 last deglaciation. We therefore explore simulations with a larger excess ice volume at the
407 Last Glacial Maximum and greater ice loss through the deglaciation in Extended Data
408 Fig. 1.

409 NH ice-cover variations were prescribed in the global sea-level model using five
410 different ice histories: Three global ice histories, ICE5G[27], ICE6GC[31] and the ANU
411 model[30], and two histories with GLAC1D reconstructions[29] over North America and
412 Greenland, and ICE5G elsewhere. These ice history reconstructions are widely used,
413 cover the whole time period under consideration and are constrained by glacial isostatic
414 adjustment modeling and a suite of sea-level and ice-cover records.

415 Elastic and density structure of the solid Earth in the sea-level model is prescribed
416 from the Preliminary Reference Earth Model (PREM)[49]. Two different models of the
417 viscosity structure of the Earth's mantle are adopted in the simulations. Figures in the
418 main text show results using the 'LVZ' model representative of structure beneath the
419 West Antarctic. The model is characterized by a 50-km thick lithosphere, a low viscosity
420 zone of 10^{19} Pa s extending from the base of the lithosphere to 200 km depth, and a
421 viscosity set to 2×10^{20} Pa s and 3×10^{21} Pa s in the remaining the upper mantle and in the

422 lower mantle, respectively. The LVZ model was adopted in refs. [28] and [36] Additional
423 simulations in Extended Data Fig. 1 adopt a viscosity structure that falls within a range of
424 models that best fit a suite of observations related to glacial isostatic adjustment[30,50]. The
425 model, labeled 'HV', has a lithospheric thickness of 120 km and upper and lower mantle
426 viscosities of $5x10^{20}$ and $5x10^{21}$ Pa s, respectively.

427 The ice-sheet model is run on a polar stereographic projection with a 20-km grid
428 resolution, while sea-level calculations are performed up to spherical harmonic degree
429 512. To couple the models, the ice-sheet model first computes changes in Antarctic ice
430 thickness over a 200 year 'coupling interval' (sensitivity tests described in ref. [26] show
431 that this choice is sufficiently short for ice-age simulations). These AIS changes are then
432 combined with NH ice cover (which is either fixed at its configuration at 40 ka
433 throughout the run for "fixed NH ice" simulations, or evolves according to the chosen ice
434 history in "evolving NH ice" simulations; See also Extended Data Fig. 8) over this
435 interval, and the combination is used as input to the sea-level model to compute the
436 associated global changes in sea level. The predicted sea-level changes, which are
437 equivalent to the negative of topography or bedrock elevation changes, are passed back to
438 the ice-sheet model and used to update bedrock topography in Antarctica. The ice-sheet
439 model then proceeds forward across another coupling interval and the process repeats
440 over the full 40-kyr simulation. Initial conditions of the ice sheet at 40 ka are provided by
441 a longer, full glacial cycle run of the ice-sheet model along with bedrock deformation
442 given by a simpler Elastic Lithosphere Relaxed Asthenosphere (ELRA) model[51]. Global
443 topography and bedrock elevation in Antarctica at the start of the simulation at 40 ka are
444 initially unknown and determined through an iterative procedure in which the predicted

modern topography at the end of a 40 ka simulation is compared to observed topography (ETOPO2, ref. [52] globally and Bedmap2, ref. [32]) in Antarctica and the difference between the two is used to correct the initial topography at 40 ka in the next iteration. The process is repeated four times, which guarantees sufficient convergence of predicted and observed modern topography.

Iceberg Alley sites and IBRD record

Sample-based investigations concentrated on deep-sea cores retrieved in the Scotia Sea's Iceberg Alley during Marion Dufresne II cruise 160 in March 2007. Sites MD07-3133 (57°26'S, 43°27'W; 3101 m water depth; 32.8 m long) and MD07-3134 (59°25'S, 41°28'W; 3663 m water depth; 58.2 m long) originate from the northern end of Dove Basin and Pirie Bank, respectively.

The age models of sites MD07-3133 and MD07-3134 are based on distinct dust-climate couplings between Southern Ocean sediment and the Antarctic EPICA Dronning Maud Land (EDML) ice core[53] on the EDML1 age model[54], which appears more consistent with local ash layer correlations than the later AICC 20102 age model[55,56], which relies on interhemispheric methane correlation. Comparison between age models (Extended Data Fig. 9c) shows older ages for the AICC 2012 age scale. Differences are minimal for the mid to late Holocene. At the time of MWP-1B the difference is on the order of 150 years, whereas it is 350 years during MWP-1A and ~500 years at LGM. This means that for AID event 2 the shift is very small and the event aligns well with MWP-1B regardless of the age model. AID event 6 would extend from ~14.3–15.2 ka in AICC 2012, a range that still encompasses MWP-1A (14.65-14.3 ka), especially within

the uncertainties of the ice-core age models, which increase from a few centuries for the time of MWP-1B up to millennium for the last glacial maximum[55,56]. Therefore, the correlations we make here and the conclusions we draw hold regardless of the age model applied.

The use of magnetic susceptibility as well as Ca and Fe records measured through X-ray fluorescence is considered a well-established approach to study coherent and synchronous changes in dust deposition across much of the Southern Ocean and the AIS across the last deglaciation[4] as well as on longer, glacial-to-interglacial times scales[57,58].

IBRD counting was conducted every centimeter on x-radiographs taken from 1-cm thick slices that were cut out from the center of each core segment and exposed to an x-ray system. The transitions from low to high and high to low IBRD contents form the basis of our AID event classification. The counting interval of 1 cm translates into 8–17 years resolution for AID 1–7, depending on the time interval and core. The IBRD data is presented here is a stack of Sites MD07-3133 and MD07-3134 to obtain a regional rather than a local record for the time 20–0 ka. It is combined from previous publications for the period 27–7 ka[4] and 8–0 ka[24]. This new IBRD stack with the EDML1 and AICC 2012 age models along with uncertainty calculations are shown in Extended Data Fig. 9c and three tables containing the IBRD data on both age scales, the age-scale tie points, and the uncertainty calculations can be downloaded from the PANGAEA data server (see link in Data Availability).

Comparison to Cosmogenic Exposure Age Data

In Fig. 4 and Extended Data Figs. 10-11, we compare modeled ice loss history in the Ross and Weddell Sea regions to records of ice thinning from cosmogenic exposure age data from ref. [35], also discussed in ref. [59]. Records at Site 1 in the Ross Sea (Fig. 4) and at Sites 11-15 in the Weddell Sea region (Extended Data Fig. 10 are consistent with the earlier deglaciation predicted in simulations that include a NH sea-level forcing. While exposure age data at Sites 3-5 (Extended Data Fig. 11a) appear to be more consistent with a later deglaciation, these sites are just outside of the region of significant ice loss in the simulation (Extended Data Fig. 11d, e). The sites are geographically close to Site S, but they exhibit substantially less thinning than the rest of the Ross Sea region (compare ice loss at red and blue stars in Extended Data Fig. 11e). Thinning rates and timing at Sites 1 and S, on the other hand, are comparable (Extended Data Fig. 11and Fig. 4b of the main text) and more representative of regional-scale ice loss that occurs in the model during the main part of the deglaciation. Taken into consideration with the Ross Sea grounding line record[7], it is possible that major deglaciation ends in this sector of the Ross Sea by around 8 ka and the thinning rates observed at Sites 3-5 indicate smaller magnitude, late Holocene ice changes. Higher resolution ice sheet modeling would be needed to investigate this issue further, which is infeasible in the long timescale coupled models described in the current study.

Data Availability

The datasets generated in this publication are available both within the PANGAEA data base system (https://doi.pangaea.de/10.1594/PANGAEA.919498) (doi:10.1594/PANGAEA.919498) and as source data for Extended Data Figure 9. The

513 modeling results are available at the following OSF database:

514 https://osf.io/g5ur2/?view_only=8acbf1e38c184d9c8f09811c8bbef036

515

516 **Code Availability**

517 The coupled ice sheet – sea level model used in this manuscript has been reported in

518 refs.[26] and [28], with the PSU-3D ice sheet model reported in the following reference:

519 https://doi.org/10.5194/gmd-5-1273-2012. The ice model is available upon request from

520 the developer, David Pollard, and the sea level model is available from Jerry Mitrovica.

521

522 **Acknowledgements**

523 The contributions of N.G. and H.K.H. were supported by the Natural Sciences and

524 Engineering Research Council (NSERC), the Canada Research Chair's program and the

525 Canadian Foundation for Innovation, M.E.W. by the Deutsche Forschungsgemeinschaft

526 (DFG grant numbers We2039/8-1 and We 2039/17-1), and J.X.M. by NASA grant

527 NNX17AE17G and Harvard University. We thank Gabriel Tseng for assistance with

528 exploratory research that informed this study, and David Pollard for insight on and use of

529 the PSU ice sheet model.

530

531 **Author Contributions**

532 N.G. contributed the numerical modeling and analysis, H.K.H. prepared model input,

533 M.E.W contributed IBRD records and together with P.U.C. and J.X.M. other published

534 data and related discussion, and all authors contributed to developing the idea and writing

535 and refining the manuscript.

Author Information

Correspondence should be addressed to Natalya Gomez (natalya.gomez@mcgill.ca).

Competing interests

The authors declare no competing interests.

References for Methods:

36 Gomez, N., Pollard, D. & Holland, D. Sea-level feedback lowers projections of future Antarctic Ice-Sheet mass loss. *Nature Communications* **6**, 8798, doi:10.1038/ncomms9798 (2015).

37 Pollard, D. & DeConto, R. M. Description of a hybrid ice sheet-shelf model, and application to Antarctica. *Geoscientific Model Development Discussions* **5**, 1077-1134, doi:10.5194/gmdd-5-1077-2012 (2012).

38 Kendall, R. A., Mitrovica, J. X. & Milne, G. A. On post-glacial sea level - II. Numerical formulation and comparative results on spherically symmetric models. *Geophysical Journal International* **161**, 679-706 (2005).

39 Gomez, N., Mitrovica, J. X., Tamisiea, M. E. & Clark, P. U. A new projection of sea level change in response to collapse of marine sectors of the Antarctic Ice Sheet. *Geophysical Journal International* **180**, 623-634, doi:10.1111/j.1365-246X.2009.04419.x (2010).

40 MacAyeal, D. R. Large-scale ice flow over a viscous basal sediment: Theory and application to ice stream B, Antarctica. *Journal of Geophysical Research: Solid Earth* **94**, 4071-4087, doi:10.1029/JB094iB04p04071 (1989).

41 Hutter, K. Theoretical glaciology: material science of ice and the mechanics of glaciers and ice sheets, Reidel Publ. *Co., Dordrecht* (1983).

42 Pattyn, F. *et al.* Grounding-line migration in plan-view marine ice-sheet models: results of the ice2sea MISMIP3d intercomparison. *Journal of Glaciology* **59**, 410-422, doi:10.3189/2013JoG12J129 (2013).

43 Pollard, D. & DeConto, R. M. A simple inverse method for the distribution of basal sliding coefficients under ice sheets, applied to Antarctica. *The Cryosphere* **6**, 953-971, doi:10.5194/tc-6-953-2012 (2012).

44 Pattyn, F. Sea-level response to melting of Antarctic ice shelves on multi-centennial time scales with the fast Elementary Thermomechanical Ice Sheet model (f.ETISh v1.0). *The Cryosphere Discussions*, 1-52, doi:10.5194/tc-2017-8 (2017).

45 Tsai, V. C., Stewart, A. L. & Thompson, A. F. Marine ice-sheet profiles and stability under Coulomb basal conditions. *Journal of Glaciology* **61**, 205-215 (2015).
46 Le Brocq, A. M., Payne, A. J. & Vieli, A. An improved Antarctic dataset for high resolution numerical ice sheet models (ALBMAP v1). *Earth System Science Data Discussions* **3**, 195-230, doi:10.5194/essdd-3-195-2010 (2010).
47 Lisiecki, L. E. & Raymo, M. E. A Pliocene-Pleistocene stack of 57 globally distributed benthic δ 18O records. *Paleoceanography* **20**, doi:10.1029/2004PA001071 (2005).
48 Liu, Z. *et al.* Transient simulation of last deglaciation with a new mechanism for Bolling-Allerod warming. *Science* **325**, 310-314, doi:10.1126/science.1171041 (2009).
49 Dziewonski, A. M. & Anderson, D. L. Preliminary reference Earth model (PREM). *Physics of the Earth and Planetary Interiors*, 1-60 (2011).
50 Mitrovica, J. X. & Forte, A. M. A new inference of mantle viscosity based upon joint inversion of convection and glacial isostatic adjustment data. *Earth and Planetary Science Letters* **225**, 177-189 (2004).
51 Huybrechts, P. & de Wolde, J. The dynamic response of the Greenland and Antarctic ice sheets to multiple-century climatic warming. *Journal of Climate* **12**, 2169-2188 (1999).
52 National Geophysical Data Center, NOAA. *2-minute Gridded Global Relief Data (ETOPO2) v2.* , 2006).
53 Weber, M. E. *et al.* Dust transport from Patagonia to Antarctica - A new stratigraphic approach from the Scotia Sea and its implications for the last glacial cycle. *Quaternary Science Reviews* **36**, 177-188, doi:10.1016/j.quascirev.2012.01.016 (2012).
54 Ruth, U. *et al.* "EDML1": a chronology for the EPICA deep ice core from Dronning Maud Land, Antarctica, over the last 150 000 years. *Climate of the Past* **3**, 475-484 (2007).
55 Veres, D. *et al.* The Antarctic ice core chronology (AICC2012): an optimized multi-parameter and multi-site dating approach for the last 120 thousand years. *Clim. Past* **9**, 1733-1748, doi:10.5194/cp-9-1733-2013 (2013).
56 Bazin, L. *et al.* An optimized multi-proxy, multi-site Antarctic ice and gas orbital chronology (AICC2012): 120–800 ka. *Clim. Past* **9**, 1715-1731, doi:10.5194/cp-9-1715-2013 (2013).
57 Lamy, F. *et al.* Increased dust deposition in the Pacific Southern Ocean during glacial periods. *Science* **343**, 403-407, doi:10.1126/science.1245424 (2014).
58 Martínez-García, A. *et al.* Iron Fertilization of the Subantarctic Ocean During the Last Ice Age. *Science* **343**, 1347-1350, doi:10.1126/science.1246848 (2014).
59 Small, D., Bentley, M. J., Jones, R. S., Pittard, M. L. & Whitehouse, P. L. Antarctic ice sheet palaeo-thinning rates from vertical transects of cosmogenic exposure ages. *Quaternary Science Reviews* **206**, 65-80 (2019).

EXTENDED DATA FIGURE CAPTIONS

Extended Data Figure 1: Sensitivity of results to ice and Earth model parameters. (a) Changes in Antarctic ice volume predicted in simulations with evolving (solid lines) and fixed (dashed lines) NH ice mass and the LVZ ("low viscosity zone") Earth model (see Methods). Blue lines are identical to those in Fig. 2b of the main text, adopting a basal sliding coefficient of 10^5 m a^{-1} Pa^{-2}, while red lines adopt a basal sliding coefficient for a stickier marine bed of 10^6 m a^{-1} Pa^{-2}. (b) As in (a) but adopting the HV ("high viscosity") Earth model (see Methods). Black dotted lines and right-hand-side y-axis in each frame show changes in NH ice volume, in meters of global mean sea level equivalent (GMSLE), prescribed in the ICE5G[27] ice history. For reference, blue and red vertical bands in (a) and (b) represent the timing of MWP and AID events as described in Figure 2a and 2c of the main text, respectively.

Extended Data Figure 2: Evolution of Antarctic ice cover with and without NH sea-level forcing. Columns: Thickness of grounded ice in meters and extent of ice shelves at 30 ka, 20 ka, 10 ka and the modern as labeled, predicted from simulations that include variations in the NH ice sheets represented by the ICE5G[27] ice history (row a) and simulations in which ice cover in the NH remains fixed (row b). Black lines in rows (a) and (b) show the grounding lines. Row c shows the difference in grounded ice thickness between simulations in rows (a) and (b), representing the impact of sea-level changes associated with NH ice sheets on the evolution of the AIS. Green and black lines represent the positions of the grounding lines with (row a) and without (row b) the NH sea-level forcing included.

Extended Data Figure 3: Influence of NH sea-level forcing on Antarctic ice cover during the deglaciation. Differences in thickness of grounded ice at the indicated times, in meters, between simulations that include variations in the NH ice sheets from ICE5G[27] ice history and in which ice cover in the NH remains fixed throughout the simulation. Differences are displayed as in Fig. 3c of the main text, but every 1 ky for the last 20 ka. Green and black lines represent the positions of the grounding lines with and without the NH sea-level forcing included, respectively.

Extended Data Figure 4: Antarctic ice volume changes in the Ross and Weddell Sea sectors. (a) Changes in ice volume in the Ross Sea sector predicted in simulations with fixed (red line) and evolving (black line) NH ice from the ICE5G ice history. (b) As in frame (a) but for the Weddell Sea sector. (c) Blue lines outline the areas included in the calculations in frames (a) and (b), and background colors indicate the change in ice thickness in meters from 20 ka to the modern in the simulations that includes NH ice cover changes from ICE5G[27].

Extended Data Figure 5: Influence of NH sea-level forcing on rate of Antarctic ice loss. (a-e) Rate of change of Antarctic ice volume, including grounded and floating ice, calculated with a 100 year running mean, predicted from simulations including (black lines) and excluding (red lines) NH ice-cover changes, using the ice histories indicated in

the legend (see Methods). Note that Fig. 3a of the main text shows the mean and standard deviation of these five frames.

Extended Data Figure 6: Patterns of sea-level change for Antarctic ice loss during MWP-1A and the early Holocene. (a-b) Predicted sea-level change, normalized by the global mean sea-level equivalent (GMSLE) associated with Antarctic ice loss during (a) MWP-1A and (b) the early Holocene including MWP-1B. Calculations are associated with simulations that include a NH forcing given by ICE5G[27]. The patterns of sea-level change and the GMSLE used in the normalization are calculated over the time windows given by the grey bands in Fig. 3a of the main text. Green and magenta stars indicate locations of far-field relative sea-level records in Tahiti and Barbados.

Extended Data Figure 7: Sensitivity of the Weddell Sea sector to geographic variability in sea-level forcing. (a) Change in ice thickness predicted from a simulation adopting the ICE5G[27] ice history in the NH that includes geographically variably sea-level changes associated with gravitational, deformational and Earth rotational effects activated by ice-cover changes globally during MWP-1A from 14.5-13.5 ka. Grey and black lines in (a) indicate the grounding-line position at the start and end of the time interval, respectively. This frame is the same as Fig. 3b of the main text but zoomed in on the Weddell Sea region where geographically variable sea-level changes associated with NH ice loss are largest (see Fig. 1c). (b) The difference between (a) and the same calculation adopting the simulation with globally uniform sea-level change from the NH. The black line in (b) is as in frame (a) and the blue lines indicates the grounding-line position at the end of the time interval for the uniform sea-level simulation. (c) Antarctic ice volume variations from simulations with geographically variable (black line) and uniform (red line) sea-level changes associated with NH ice loss over the MWP-1A interval. Frames (d-f) are as in (a-c) but for the early Holocene interval from 11.5-9 ka. In this case, frame (d) is as in Fig. 3d of the main text but zoomed in on the Weddell Sea region. Note that the uniform sea-level change is calculated relative to modern topography, and scaled such that the total contribution to eustatic sea-level change from the NH over the last deglaciation from 21 ka on is 95.5 meters, in agreement with ref. [27].

Extended Data Figure 8: Predicted Antarctic ice volume changes and GMSLE contributions. (a) Changes in AIS volume predicted in a simulation with NH ice cover fixed at the 40 ka configuration within ICE5G[27] (solid red line), and in simulations with evolving NH ice adopting the ICE5G[27] (solid black line), ICE6GC[31] (dashed black line) and the ANU[30] model (cyan line) ice histories, as well as two composite ice histories in which ice cover over North America and Greenland in ICE5G has been replaced by regional GLAC1D[29] models (blue lines). Finally, the dashed red line represents a simulation in which the NH ice sheets are fixed at the modern configuration rather than at the 40 ka configuration throughout the simulation. In this case, marine-based sectors of the AIS start on even shallower bedrock, and hence the predicted ice sheet growth is larger at the Last Glacial Maximum, while the ice loss during the deglaciation occurs later and is of even smaller magnitude than in the original simulation. Note that this is not a realistic starting configuration. Frame (b) is as in frame (a) but expressed as a GMSL equivalent relative to the modern state. This is calculated by taking the ice above

floatation thickness in Antarctica relative to the paleo bedrock topography at each time step in the model, and dividing by the area of the modern ocean. Note that frames (a) and (b) are not directly proportional because as the bedrock topography in Antarctica evolves the volume of ice above floatation in marine sectors also changes. Blue and red vertical bands in (a) and (b) represent the timing of MWP and AID events as described in Figure 2a and 2c of the main text, respectively.

Extended Data Figure 9: Age model comparison and uncertainty for IBRD flux record from Iceberg Alley. (a) Age difference between the AICC 20102 age model[55,56] and EDML1 age model[54]. (b) Age uncertainty in the AICC 2012 age model. (c) IBRD flux time series adopting the AICC 2012 (black line, as in Figs. 2c and 4b of the main text) and EDML 1/EDC 3 (blue line) age scales. The IBRD stack is composed of records from Sites MD07-3133 and MD07-3134. It is presented here for the time 20–0 ka and was combined from previous publications for the period 27–7 ka[4] and 8–0 ka[24]. Vertical brown bars indicate AID 1-7[4] on the AICC 2012 age scale. Blueish vertical bars indicate the times of MWP-1A[21] and MWP-1B[22]. Horizontal black error bars at the top of frame (c) show propagated uncertainties for the upper and lower bounds of each AID event for errors in tie point correlation to EDML[4] and uncertainties of the AICC 2012 age model.

Extended Data Figure 10: Comparison of predicted and observed ice thickness changes in the Weddell Sea region. (a-b) Predicted (lines) and observed (error bars) ice thickness above modern thickness in meters at (a) Sites 11-13 and (b) Sites 14-15 from ref. [35]. (c) Map of predicted ice thickness at 12 ka in the simulation with ICE5G[27] with locations of the sites discussed in the Weddell Sea and Ross Sea (see Extended Data Figure 10) as indicated. Predictions are from simulations in which NH ice cover is evolving according to ICE5G[27] (black lines) and fixed (blue lines), respectively. Error bars show cosmogenic exposure age data with 2σ uncertainty from ref. [35]. See Methods section for further discussion of these results.

Extended Data Figure 11: Comparison of predicted and observed ice thickness changes in the Ross Sea region. (a) Predicted (lines) and observed (2σ error bars) ice thickness above modern thickness in meters at Scott Coast Site S discussed in the main text and at Sites 1 (red) and 3-5 (shades of blue) from ref. [35]. Locations of the sites are indicated on the maps in frames b-e. Predictions are from simulations in which NH ice cover is evolving according to ICE5G[27] (solid lines) and fixed (dashed lines), respectively. Observations are cosmogenic exposure age data from ref. [35]. Red vertical bands represent the timing of AID events 1 and 2 as described in Fig. 2c of the main text. (b) Map of predicted ice thickness at 12 ka in the Ross Sea in the simulation with ICE5G[27]. (c-e) The difference in ice thickness between 12 ka (frame b) and 11, 10, and 9 ka, respectively. See Methods for further discussion of these results.